Experimental cross sections for electron-impact ionization of iron ions: Fe^{5+}, Fe^{6+}, and Fe^{9+}

D. C. Gregory and F. W. Meyer
Physics Division, Oak Ridge National Laboratory, Oak Ridge, Tennessee 37831-6372

A. Müller*
Joint Institute for Laboratory Astrophysics, University of Colorado and National Bureau of Standards, Boulder, Colorado 80309

P. Defrance
Université Catholique, Louvain la Neuve, Belgium
(Received 14 May 1986)

Absolute cross sections have been measured for electron-impact ionization of Fe ions of initial charges 5+, 6+, and 9+ from below threshold to 1500-eV collision energies. Distorted-wave calculations including only direct ionization from ground-state ions underestimate the measured peak cross sections by 60—70% due to the effects of metastable states and contributions of excitation autoionization to the total cross sections. Ionization rate coefficients and fitting parameters are presented for this data and for Fe^{+} and Fe^{2+}.

I. INTRODUCTION

Knowledge of basic atomic processes is vital to the understanding of stellar, interplanetary, and laboratory plasmas.[1,2] The accuracy of modeling power balance, impurity radiation profiles, and charge-state distributions depend critically on knowledge of ionization, excitation, and recombination cross sections for a wide range of charge states of all elements found in the plasma.[3,4] Modeling programs depend on scaling laws,[5] more accurate specific calculations (where available), and benchmark measurements to provide the required large database.

The most commonly used source of electron-impact ionization cross section in plasma modeling codes is the semiempirical Lotz formula.[6] For ions of initial charge 3+ and lower, a three-parameter formula is suggested,[7,8] while ionization of ions with initial charge 4+ and higher is described by the very simple formula

$$\sigma(E)=4.5\times10^{-14}\sum_j \frac{r_j}{I_j E}\ln\left[\frac{E}{I_j}\right], \quad (1)$$

where the cross section $\sigma(E)$ in cm^2 is dependent only on the energy E (in eV) and on the number of electrons (r_j) and ionization threshold energies (I_j, also in eV) of the (j) subshells to be summed over. The Lotz formula is based on Coulomb-Born theory for infinite-Z projectiles and on a number of measurements for singly charged ions. It is intended to account only for the process of direct knockout of a target electron by the incident projectile electron, and agreement with experiment for direct ionization is usually well within the accepted accuracy of a factor of 2 where direct comparisons can be made.

There are, however, other processes which may lead to ionization. The indirect ionization process of excitation of an inner-subshell target electron followed by autoionization of the resulting excited ion was predicted[9] and observed[10] in 1968. This process, commonly known as excitation autoionization, has been extensively studied in the last decade, and has been found to range in importance from negligible to dominant compared to direct ionization. A number of systematic studies of isoelectronic[11,12] (same number of electrons) and isonuclear[13–15] (same element) systems have led to the general observation that *indirect* ionization effects become more important with increasing charge and increasing Z. In certain cases, however, the upper levels of transitions leading to large enhancements of the ionization cross section may become bound as the charge or Z increases and a sudden decrease in this contribution to the cross section may be found.[16] Detailed knowledge of the energy levels of the target ion and specific quantal cross-section calculations have in many cases proven successful in explaining or predicting experimental results.

Most previous systematic studies of electron-impact ionization have concentrated on the light elements or the more conveniently and easily produced ions of noble gases.[17] Due to the difficulty in producing multiply charged metal ions in sufficient quantities for beam experiments, the only metals for which crossed-beam experiments have been performed for each of the first three charge states are titanium[16,19,19] and antimony,[20,21] although two of the first three charge states have also been studied for several other metals (see, for example, Refs. 20 and 21). No results have been published for an electron-ion crossed-beam experiment involving any metal ion of initial charge state higher than 3+.

Iron ions are abundant in the solar corona[22] and iron is often cited as the most common heavy impurity in large plasma research devices made of stainless steel,[23,24] but ionization measurements have heretofore only been made for Fe^{+} and Fe^{2+} (Refs. 25 and 19, respectively), using the crossed-beam technique. As part of a continuing sys-

tematic study of electron-impact ionization of ions we present here cross sections for a series of iron ions in initial charge states $5+$, $6+$, and $9+$. These charge states are intermediate between the very low charges that have been studied by crossed-beam methods in the past and the higher charges which are more accessible to plasma rate measurements. These ions have also been investigated theoretically and the results are presented in the accompanying paper.[26] We were unable to measure accurate absolute cross sections for ionization of Fe^{7+} and Fe^{8+} because of contamination of the incident ion beams by impurities with the same m/q.

We discuss the experimental arrangement in Sec. II, followed by an evaluation of the uncertainties in Sec. III, the presentation of the results with some discussion in Sec. IV. Since many users of such data are interested in Maxwellian ionization rate coefficients in addition to cross sections, Sec. V presents results of rate-coefficient calculations based on the present cross-section measurements. Finally, a summary of this work is presented in Sec. VI. The Appendix discusses fits to the rate-coefficient calculation.

II. EXPERIMENTAL ARRANGEMENT

Extensive discussions of the techniques of experiments with crossed electron and ion beams are available,[27] and many details of this apparatus and associated uncertainties have been published.[28,29] However, the recent development of a new postcollision analyzer, which is used for the first time in this experiment, requires some discussion. The previous apparatus and uncertainty descriptions may be considered as background material, and those aspects which have not been modified (such as the electron gun, beam-overlap measurement and evaluation, and precollision ion optics) will be only briefly described here. Rather, the present paper will emphasize the postcollision beam transport, diagnostics, and uncertainties.

Absolute measurements of electron-impact ionization cross sections are difficult both because of the problems in measuring the necessary absolute quantities[30] and because of the low signal level compared to the intensities of the incident beams. For beams crossing at 90°, the cross section is related to the signal count rate through the equation

$$\sigma(E)=\frac{Rqe^2v_iv_e}{I_iI_e(v_i^2+v_e^2)^{1/2}}\frac{F}{D}\ , \tag{2}$$

where R is the signal count rate, q is the charge on the incident ion, e is the charge on an electron, v_i and v_e are ion and electron velocities, I_i and I_e are the ion- and electron-beam currents, D is the probability of detecting and counting a signal event, and F is the form factor which takes into account the overlap of the ion and electron beams. The form factor is calculated from beam profiles through the relation

$$F=\frac{\int I_i(z)dz\int I_e(z)dz}{\int I_i(z)I_e(z)dz}\ , \tag{3}$$

where $I_i(z)$ and $I_e(z)$ are the measured beam intensity profiles and the z direction is perpendicular to both beams. Each quantity which enters into Eq. (2) must be carefully and independently measured in order to assure an accurate absolute cross section. In addition, the signal count rate must be determined in the presence of a background which comes from ionizing collisions of the incident ion beam with residual gas in the interaction chamber. Other potential sources of counts in the signal channel include aperture scattering and spatial modulation of the ion beam (or of the signal ion component of the ion beam) by the space charge of the electron beam.

The traditional technique of determining the background level in beam experiments is by chopping one or both beams and separately counting background and signal-plus-background events.[31] An alternative method introduced by Brouillard and Defrance[32] involves sweeping one beam through the other while collecting events in a time-based multichannel analyzer (MCA). The latter method measures background and signal-plus-background in different bins of the MCA and replaces the determination of a form factor by the generally less difficult measurement of sweep velocity. The traditional beam-chopping technique is employed in the present experiment, and since no background events are produced in the detector by the electron beam alone, only the electron beam need be chopped. A necessary test for the absence of space-charge modulation of the ion beam, which may contribute an apparent positive or negative cross section depending on the geometry and relative sensitivity of the detector, is the measurement of zero cross sections below the threshold for any process which can be detected. It has been aptly said for many years that the most important points one measures are the ones below threshold.[33] No apparent cross section was observed below threshold for any of the ions studied here.

A. Ion source

Multicharged ion sources based on electron-cyclotron-resonance (ECR) heating have been shown to produce reliable, stable dc beams suitable for crossed-beam experiments. They generally require little maintenance and produce larger currents of highly charged ions than the Penning-ion-gauge (PIG) source[34] which has been utilized for previous experiments in this laboratory. Accordingly, the Oak Ridge National Laboratory (ORNL) ECR ion source was developed to extend the beam species and charge states available for a variety of atomic physics experiments. The ion source development and initial testing, a well as a description of vital design parameters, have been reported by Meyer.[35]

The combination of an extremely wide range of electron energies produced in the vicinity of the ECR surface and low neutral density in the source second stage allows the extraction of a wide range of charge states from the source with very little change in source tuning parameters. Under these conditions it may be assumed that, except perhaps near the upper limit of the charge-state distribution, any metastable levels will be populated and a statistical population of all states which live long enough (in the

microsecond to millisecond range) will be present in the ion beam. In these experiments, the observed ionization onsets correspond to the expected thresholds for ionization of ground-state ions except for Fe^{9+}, where the experimental ionization threshold is 50 eV below that of ground-state ions.

B. Ion-beam optics

After extraction of the ions from the source (at 5-kV accelerating voltage for this set of experiments), the beam is analyzed in a stigmatic 90° magnetic charge analyzer having a 40-cm radius of curvature. Adjustable slits at the magnet object and image positions allow variation of the mass resolution and beam collimation. The analyzing magnet was operated in this experiment with sufficient resolution to separate the various isotopes of iron. Additional steering and focusing elements downstream of the magnet are used to maximize beam transmission into the ultrahigh-vacuum chamber. Differential pumping in the beam line reduces the pressure from the operating pressure of the ion source second stage, about 2×10^{-6} Torr, to approximately 6×10^{-9} Torr in the final chamber of the beam line. The main crossed-beam interaction chamber is maintained at a pressure of approximately 2×10^{-9} Torr with beams present.

Ions entering the main interaction chamber, shown in Fig. 1, pass through one-dimensional einzel lenses which include vertical and horizontal steering. Beam transmission may be checked at a Faraday cup located behind the charge purifier, if the purifier deflector voltage is set to zero. With positive voltage applied to the back plate of the purifier, the ion beam is deflected by 90°, removing any ions that have changed charge along the flight path from the source analyzing magnet. An aperture located 1 cm past the purifier exit is the limiting aperture (0.3×0.7 cm^2) in the chamber, and minimizing current lost to this aperture is a convenient diagnostic to assure maximum transmission of ions to the collision volume. The vertical ion-beam intensity profile was measured at the center of the collision volume, located in the middle of the electron gun. Deflection of the beam produced by the perpendicular magnetic field which confines the electron beam is corrected by vertical deflectors located immediately before and after the collision box. All apertures downstream of the collision volume are large enough to pass the ion beam without restriction, and 100% transmission is found from the collision volume to both the primary ion-beam cup and the signal detector. The einzel lens downstream from the electron gun is used during diagnostics only, although some vertical beam deflection at this point is used to correct any slight misalignment of the detector analyzing magnet.

The analyzing magnet shown in Fig. 1 is double focusing and has a radius of curvature of 20 cm. The signal ions which have been ionized in the collision volume are deflected 90° and imaged into the signal channel. Horizontal steering is provided at the entrance to the signal channel near the detector and a 90° electrostatic analyzer deflects the signal ions out of the magnet dispersion plane. The electrostatic deflection is in the vertical direction, although it is shown to be horizontal in Fig. 1 for ease of presentation. A small Faraday cup located behind the vertical deflector back plate may be used in diagnostic tests. The detector is a channel electron multiplier with a 1-cm-diam cone, and is operated with the front cone at a potential of -3 kV. A cover plate immediately in front

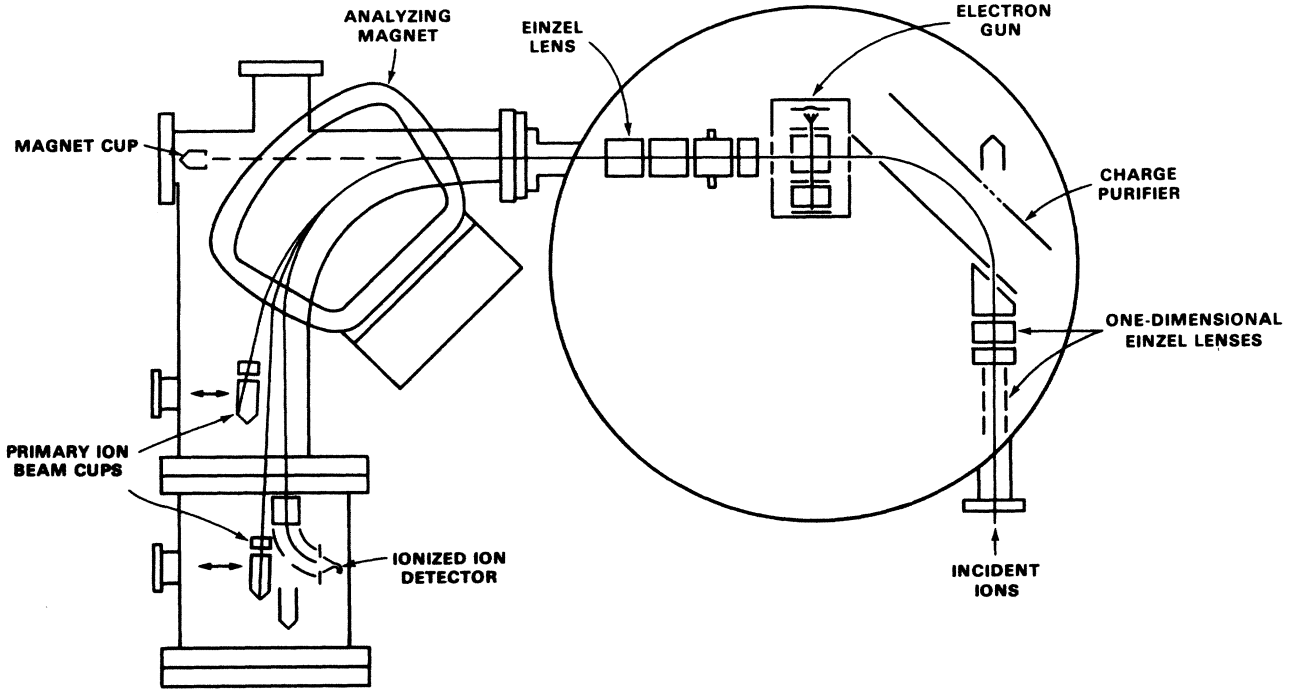

FIG. 1. Schematic of the crossed-beam collision chamber and postcollision magnetic charge analyzer.

of the detector may be biased to control the electric field near the detector cone.

With ionized ions centered in the signal channel, the primary ion beam is deflected through an angle less than 90° by the analyzing magnet and is collected in one of two movable Faraday cups, depending on the ratio of incident charge to the charge of the signal ions. The ratios of incident-to-ionized ion charge states that can be studied in the present arrangement range from $\frac{5}{6}$ to $\frac{15}{16}$. This range is limited by the movement restrictions of the Faraday cups for low charge states and by the necessity of cleanly separating primary and signal ion channels for high charge states. In the present experiment, the front cup (closest to the analyzing magnet) was used to collect incident Fe^{5+} and Fe^{6+} ion beams while the back cup was used for the Fe^{9+} beam. Typical ion-beam currents (electrical) in this experiment were 80 nA of Fe^{5+}, 100 nA of Fe^{6+}, and 120 nA of Fe^{9+}.

C. Electron beam

The electron gun used in this experiment is very similar to the design by Taylor *et al.*[36] and its characteristics have been well documented.[36,37] The beam is immersed in a 250-G magnetic field in order to confine the electrons and produce a beam of uniform rectangular cross section over the length of the collision region for a very wide range of electron energies. The electrons are accelerated from an indirectly heated planar cathode through a series of apertures in a uniform electric field to minimize spiraling. The electron collector consists of an end-on array of sharpened tantalum "razor blades" which minimize the escape of backscattered electrons, and the collector is normally biased at + 300 V or to one-half the beam energy (whichever is greater) to prevent the escape of secondary electrons from the collector region. Careful collector design not only ensures an accurate electron current measurement but is also important to prevent possible ionization of primary beam ions by backscattered or secondary electrons. For the present gun this is especially important since the axial magnetic field tends to return such electrons to the collision region. The electron beam is switched off by applying a potential to one of the gun electrodes to make it more negative than the cathode so that electrons are stopped at that point. The energy spread in the electron beam was determined by analysis of excitation cross-section measurements to be 1.5 eV at low energies,[38] and is expected to become slightly larger at higher energies. The energy spread is dominated, however, by small changes of potential across the collision volume due to nearby deflector plates. Recent modifications to the apparatus have reduced this effect and we estimate the energy spread to be 1 eV full width at half maximum (FWHM) in these experiments.

The vertical electron-beam profile is measured at the center of the collision box by scanning a probe plate having a narrow horizontal slit through the beam. The current transmitted through the slit is measured as a function of the probe position. The probe movement and current measurement are computer controlled, and beam profiles may be stored for comparison with other profiles or for form-factor calculations, for which the required integrals are approximated numerically [see Eq. (3)]. The electron gun characteristics are stable and reproducible so that stored electron profiles may be used to calculate form factors in conjunction with ion profiles taken hours or even days later. The probe may be rotated by 90° at any time so that ion profiles are measured with the same probe and slit and at the point of intersection with the electrons.

D. Diagnostics

A number of diagnostic measurements are regularly carried out, preferably at least once for each ion studied, in order to assure complete collection of the primary ion beam and ionized signal ions. These diagnostics normally consist of tuning the primary ion beam through the postcollision analyzer system, scanning signal-channel voltages while monitoring the net signal level, and the evaluation of pulse transmission in the detector electronics. In practice it is found that the signal-channel settings do not change rapidly with the m/q ratio of the ion beams and these detailed diagnostics can, with some increase in absolute uncertainty, be omitted where the signal-to-background ratio makes such scans impractical. Full diagnostic studies were carried out for each ion in this experiment.

The primary ion beam is tuned through the apparatus by sequentially centering it in the diagnostic Faraday cups found after each major beam steering element. Ions entering the main interaction chamber are first tuned into the cup located behind the charge purifier. When the charge purifier voltage is turned on, the beam is steered into the magnet cup located straight through the analyzing magnet while minimizing the current blocked by the aperture located at the electron gun entrance. The analyzing magnet can be set to bend the primary ion beam 90°, and the beam is centered in a small cup located behind the signal channel 90° electrostatic deflector. When the analyzer magnetic field (measured with a Hall probe) is reduced by the ratio of the incident ion-beam charge to the signal ion charge, the signal ions will be centered on this same line. The primary ion beam can then be captured in one of the two movable primary ion-beam cups. The appropriate cup is scanned across the beam to assure its proper centering, and measurement of current to a shield in front of the cup provides a check that all of the beam is collected by the cup. The final tests for the primary ion beam involve monitoring the beam current while varying the analyzer magnetic field and the voltage on the vertical deflectors just downstream of the interaction volume. The vertical deflection is set so that the primary ion beam is centered in the cup, and the horizontal centering of the beam must correspond to the magnet setting scaled to center the signal ions in the signal channel.

The signal ions must be centered in the channeltron detector and all ions must be detected, or a measured correction must be made for any ions which are not counted. The horizontal steerers at the entrance to the signal channel provide a convenient means of scanning the signal ion "beam" across the detector, and the 90° electro-

static deflector used to take the signal ions out of the magnetic analyzer plane may also be used to sweep the signal ions in the perpendicular plane. It has been noted that the effective active area of a channeltron depends in part on the potentials of nearby surfaces,[39] and adjusting the voltage to the cover plate immediately in front of the channeltron cone provides a means of maximizing this sensitive area. Since the background count rate may change as stray ions hit various surfaces during these three voltage scans, the net signal must be the criterion for tuning, and effectively the apparent cross section at a single electron energy must be measured at each voltage of each critical tuning element. The assumption that each of these tuning parameters is independent may be checked by repeating the diagnostic scan sequence to be sure that adjustment of downstream parameters does not effect the desired setting of the upstream tuning elements. In practice, all tunings converge to optimum settings after one or two sets of diagnostic scans.

Pulse transmission through the detector electronics is the third critical diagnostic measurement. The electron multiplier gain is determined largely by the bias voltage across it, and the amplifier gain may also be increased until just before clipping of the largest signal pulses begins. The net signal at a given electron energy is measured as a function of lowest pulse voltage counted in order to determine the pulse transmission. Extrapolation of the net signal to zero discriminator setting determines the true signal; the ratio of the signal at the discriminator cutoff used to the true signal is the pulse transmission. In the present experiments the pulse transmission was measured to be between 0.98 and 1.00.

III. UNCERTAINTIES

The individual measurements presented here are independently absolute; that is, all of the quantities in Eq. (2) are measured for each ion at each energy. The uncertainties listed in Table II and plotted in Figs. 2–4 are relative, reflecting only statistical uncertainties and variations in form factor during the measurement, in those cases where such variations are significant compared to the counting statistics. The relative uncertainties are reported at the one standard deviation (1-s.d.) level or its equivalent, and accurately represent the uncertainty in the shape of the cross-section curve and its features at that confidence level. Additional uncertainties are common to all of the measurements and are combined to form the absolute uncertainty of the entire cross-section curve.

TABLE I. Absolute uncertainties. All uncertainties are good confidence level (equivalent to 90% CL on statistical uncertainties). Uncertainties listed apply to Fe^{5+}, Fe^{6+}, and Fe^{9+}.

Source	Uncertainty (%)
Counting statistics (typical value at peak cross section at 90% CL)	±3
Form factor (total absolute uncertainty)	±4
Transmission of ions to detector	±4
Signal ion detection and pulse transmission	±3
Ion current measurement	±2
Electron current measurement	±2
Ion and electron velocities	±1
Quadrature sum	±7.8

The components of the absolute uncertainty are listed in Table I at a level equivalent to a 90% confidence level (CL) for statistical uncertainties. The dominant sources of uncertainty in this experiment are the transmission of signal ions to the detector, the detector efficiency, and systematics in the measurement of the form factor. Previous descriptions of this apparatus[28,29] have dealt with the evaluation of absolute uncertainties and despite the recent modifications, these discussions are still pertinent. A brief description of each category will therefore suffice here.

The absolute uncertainty due to counting statistics is ±3% for a typical point near the peak cross section at the 2-s.d. level, which is approximately the 90% confidence level for these measurements. In addition to the diagnostics discussed above, the ion and electron currents may be confirmed by simple tests (tuning the ion beam into an upstream cup or varying the electron collector bias) which give us confidence that these measurements are accurate, and an absolute uncertainty of ±2% has been assigned to each of these currents. Measurements of the ion and electron velocities are even more straightforward, depending only on the accelerating voltages and the absence of stray fields in the collision region, and a 1% uncertainty is allowed.

Complete transmission of ions to the detector is difficult to maintain and even more difficult to assess. The diagnostics described in Sec. II D above provide reasonable assurance that all signal ions are reaching the detector if the maximum cross section is measured over relatively broad tuning ranges of critical parameters and if the parameters can be simultaneously centered in these ideal ranges. As has been noted, such scans are time-consuming and not always possible due to low signal-to-background ratios. Slight drifts in upstream ion tuning conditions may also cause loss of complete transmission during measurements. However, repeated iterations of tuning, scans, and data collection provide 100% transmission and assurance of accurate measurements. A ±4% absolute uncertainty is allowed for transmission of ions to the detector.

The detector efficiency is assumed to be 0.98±0.02 for these ions. The only absolute measurements of the detection efficiency of channel electron multipliers of which we are aware with similar operating conditions obtained values near 100%.[39–41] Uncertainties in the pulse transmission depend on both the number of pulses lost below the discriminator level and the accuracy of the pulse-height distribution measurement. Almost all pulses (98–100%) were counted in this experiment and pulse-height distributions were measured with small uncertainties, so the product of detector efficiency and pulse transmission is assigned an absolute uncertainty of ±3%.

Form factors depend on the measurement of beam intensity profiles and on the calculation of beam-overlap integral. The principal dangers associated with the measurement of beam profiles are possible changes in the ion

beam during the profile measurements and insufficient precision in ion or electron profile measurements. Both of these effects will generally be observed as instability in the form factor and taken into account in the relative uncertainty. Electron profile measurements at high energies may be influenced by the generation of background gas due to outgassing of the probe, and some relative uncertainty is allowed for this possibility. Insufficient precision in the profile measurement and outgassing, however, are potentially systematic problems and must also be considered in the absolute uncertainty. Since beam profiles may be measured at different times and stored on the computer, calculation of the beam overlap may also be influenced by misalignment of the probe or changes in profile between the time of measurement and data collection. Frequent checks are made for each of these sources of error and a significant fraction of data collection time is spent obtaining accurate form factors for each cross-section measurement. The absolute uncertainty asigned to form-factor measurement and calculation is ±4%.

As shown in Table I, the quadrature sum of all of the uncertainties discussed above amounts to ±7.8%. This is the "good confidence level" absolute uncertainty associated with each of the three measurements reported here.

TABLE II. Experimental electron-impact ionization cross sections for Fe^{5+}, Fe^{6+}, and Fe^{9+}. Uncertainties are 1 s.d. relative only.

Fe^{5+}		Fe^{6+}		Fe^{9+}	
Energy (eV)	Cross section (10^{-18} cm^2)	Energy (eV)	Cross section (10^{-18} cm^2)	Energy (eV)	Cross section (10^{-18} cm^2)
81.5	0.04±0.12	96.6	0.06±0.23	145	0.09±0.07
91.3	−0.03±0.11	106.2	−0.14±0.23	170	−0.02±0.09
97.0	0.60±0.10	111.3	−0.17±0.24	182	0.19±0.11
99.8	1.58±0.13	116.5	0.13±0.17	194	0.04±0.06
101.9	2.75±0.19	121.2	−0.05±0.21	211	−0.05±0.08
106.8	4.57±0.17	126	0.52±0.19	219	0.23±0.07
111.8	5.84±0.16	131	1.96±0.30	243	0.42±0.05
114.7	6.61±0.16	136	2.61±0.15	268	0.52±0.05
116.9	7.07±0.15	141	4.10±0.19	293	0.96±0.04
118.7	7.30±0.15	146	4.46±0.15	318	1.13±0.05
120.6	7.48±0.15	151	5.62±0.18	343	1.38±0.04
122	7.79±0.28	155	5.65±0.27	367	1.50±0.05
126	8.74±0.29	166	6.20±0.36	392	1.64±0.05
132	9.74±0.15	176	7.08±0.26	443	1.73±0.05
136	10.41±0.26	186	7.53±0.28	492	1.80±0.03
141	11.13±0.13	195	7.70±0.08	540	1.91±0.06
146	11.45±0.11	215	8.34±0.09	565	2.03±0.07
151	12.01±0.16	235	8.76±0.09	589	1.99±0.04
156	12.43±0.12	245	9.10±0.16	639	2.04±0.04
166	12.92±0.10	255	9.03±0.09	690	2.03±0.03
176	13.32±0.11	275	9.29±0.09	740	2.04±0.04
196	14.07±0.06	295	9.50±0.05	789	2.16±0.03
216	14.17±0.13	317	9.57±0.21	839	1.97±0.06
235	15.02±0.14	342	9.69±0.15	888	2.07±0.03
255	15.21±0.13	367	9.39±0.15	992	1.95±0.16
275	15.56±0.12	391	9.45±0.10	1094	1.87±0.07
292	15.40±0.23	441	9.30±0.13	1191	1.68±0.05
317	15.48±0.06	490	9.10±0.10	1247	1.78±0.05
342	15.26±0.10	540	9.01±0.07	1299	1.65±0.05
366	14.90±0.08	589	9.03±0.06	1400	1.67±0.05
391	14.62±0.05	638	9.02±0.06	1504	1.50±0.05
415	14.51±0.04	689	8.85±0.06		
465	14.26±0.06	788	8.16±0.07		
490	14.18±0.05	888	7.79±0.05		
539	13.91±0.04	990	7.28±0.04		
588	13.69±0.03	1236	6.69±0.08		
638	13.23±0.06	1485	5.85±0.05		
688	13.05±0.05				
787	12.19±0.02				
885	11.29±0.06				
988	10.72±0.03				
1236	9.11±0.07				
1484	8.37±0.07				

IV. RESULTS AND DISCUSSION

A. Fe^{5+}

Cross sections for electron-impact ionization of Fe^{5+} are listed in Table II and plotted in Fig. 2. Relative uncertainties at the 1-s.d. level are used in both the table and the figure. The absolute uncertainty of the cross-section curve at good confidence level is $\pm 7.8\%$. The measurements are compared to results from the semiempirical Lotz formula[6] (dashed curve) and to distorted-wave calculations by Younger.[42] Both theoretical curves are intended to account only for direct ionization of $3d$ and $3p$ electrons. The predicted thresholds[42,43] for ionization of these electrons are 98.7 and 155.5 eV, respectively, and the observed onset of ionization is consistent with the predicted threshold. On this basis we conclude that the incident Fe^{5+} ion beam does not contain a significant metastable component.

Distorted-wave calculations have proven to be generally reliable as predictions of direct ionization in those cases where a straightforward comparison could be made. In this case, the peak of the experimental cross section, 15.5×10^{-18} cm^2, is approximately 60% larger than the peak cross section predicted by distorted-wave direct-ionization calculations, and the accompanying paper[26] shows that the difference is accounted for by autoionization following inner-subshell excitations of the type $3p$-nl and $3s$-nl. The enhancement of the cross section due to these processes is observed to begin at threshold and to extend to the highest energies measured here. There are no sharp features resolved in the data which might indicate the dominance of one especially strong isolated transition.

B. Fe^{6+}

The cross sections for ionization of Fe^{6+} are shown in Fig. 3 and listed in Table II. Relative uncertainties are listed in the table at the 1-s.d. level, and typical uncertainties are shown in the figure except at high energies where the uncertainties are comparable to the size of the plotted points. The observed onset of ionization is near the 124-eV threshold for removal of an outer $3d$ electron from the ground-state ion; no contribution from metastable ions is apparent.

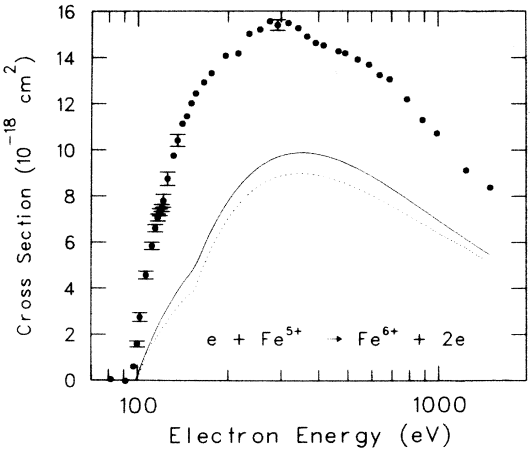

FIG. 2. Cross section vs interaction energy for electron-impact ionization of Fe^{5+}. Solid circles are the present experimental data, with 1-s.d. relative uncertainties shown. The dashed curve is the cross section predicted by the semiempirical Lotz formula (Ref. 6) and the solid curve is a distorted-wave calculation by Younger (Ref. 42), both based on direct ionization of $3d$ and $3p$ electrons.

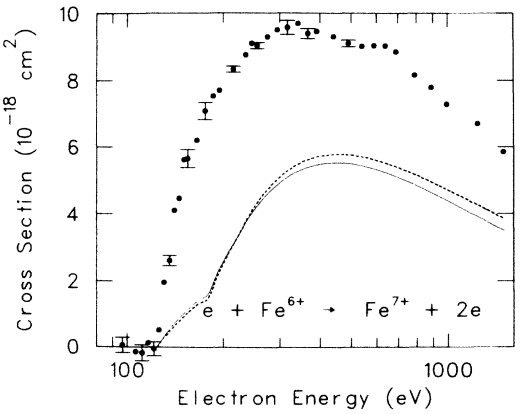

FIG. 3. Cross section vs interaction energy for electron-impact ionization of Fe^{6+}. Solid circles are the present experimental data, with representative relative uncertainties at the 1-s.d. level shown. The solid curve is a distorted-wave calculation by Younger (Ref. 42) for direct ionization of electrons from the $3d$, $3p$, and $3s$ subshells, and the dashed curve is from the Lotz formula (Ref. 6) for ionization from the same subshells.

The measurements are compared in Fig. 3 to Lotz formula results[6] (dashed curve) and to distorted-wave calculations (solid curve) for direct ionization of electrons from the $3d$, $3p$, and $3s$ subshells with thresholds[42,43] at 124, 180, and 221 eV, respectively. The calculations are consistently below the measurements with the observed peak cross section of 9.5×10^{-18} cm^2 over 70% above the predicted peak for direct ionization. As in the case of Fe^{5+}, the accompanying paper[26] ascribes this difference to autoionization following inner-subshell excitations of the types $3p$-nl and $3s$-nl. Again, no sharp onsets indicative of strong isolated transitions are found in the data, although a relatively small but broad feature is observed to onset between 550 and 600 eV. A similar, though less distinct, change in slope may be observed in the Fe^{5+} cross-section curve near 400 eV. No process has been suggested to account for these features.

C. Fe^{9+}

Cross sections for ionization of Fe^{9+} are listed in Table II, along with 1-s.d. relative uncertainties. The data are plotted in Fig. 4 with representative relative uncertainties. The uncertainty in the absolute magnitude of the curve near the peak cross section is $\pm 7.8\%$ at good confidence level. The onset of ionization is found at approximately 215 eV, well below the threshold for removal of an outer $3p^5$ electron from the ground-state ion, which is predicted to occur at 263 eV.[44] No significant change in the slope of the cross-section curve is seen at the ground-state ioni-

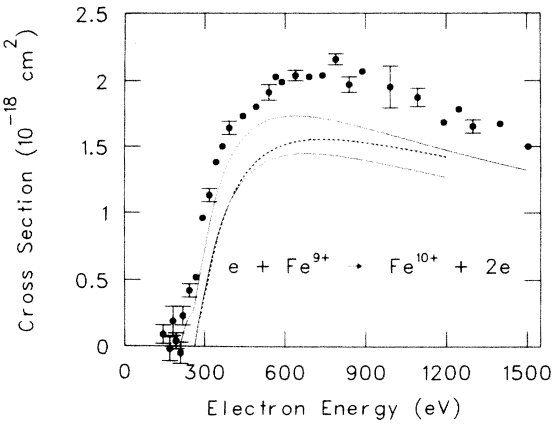

FIG. 4. Cross section vs interaction energy for electron-impact ionization of Fe^{9+}. Relative uncertainties are shown for selected energies at the 1-s.d. level. The lower solid curve is a distorted-wave calculation for direct ionization of ground-state ions (Ref. 44), while the upper solid curve is a similar calculation for ions in the $3p^4 3d$ metastable state (Ref. 26). The dashed curve is the prediction of the semiempirical Lotz formula (Ref. 6) for ionization of ground-state ions.

zation threshold, indicating that the primary Fe^{9+} ion beam is strongly dominated by a metastable configuration approximately 50 eV above the ground state.

The measurements are compared in Fig. 4 to distorted-wave calculations of direct ionization from the ground state (Ref. 44) and to similar calculations for ions initially in the $3s^2 3p^4 3d$ metastable state (from the accompanying paper—Ref. 26). Although the peak calculated cross section for ground-state ions is about 65% lower than the observed peak, the calculations for ionization of metastable ions are in good agreement with the experiment up to approximately 550 eV, and agreement continues to be reasonable at higher energies. Both calculations shown here are only for direct ionization of M-shell electrons. Additional contributions of excitation of inner-subshell electrons followed by autoionization from the metastable initial configuration, as discussed in the accompanying paper, improve the agreement somewhat at the higher energies.

D. Discussion

The ions in this study are intermediate between the low charge states of Fe for which ionization cross sections have been measured and the higher charge states such as Fe^{15+}, which has received considerable attention in theoretical studies and is predicted to be dominated by indirect ionization.[45] It is important to bridge the gap between low and high charge states in order to understand this important isonuclear sequence. In addition, the three measurements reported here provide an interesting contrast since enhancements in the cross sections are due to different mechanisms.

Both of the previous ionization measurements of Fe ions[19,25] found significant contributions from metastable components in the ion beams. The present results observe no evidence of significant metastables in the incident Fe^{5+} and Fe^{6+} beams, but metastable ions dominate the Fe^{9+} results. No predictions have been made of the possible importance of metastables for higher charge states of Fe, but such effects can be quite important depending on the energy above the ground state and possible differences in branching ratios for autoionization.

For the lower charge states of Fe, rather complicated electron configurations result when an excitation or ionization event involves an inner-subshell electron, and it is difficult to predict the importance of indirect ionization. For Fe^+ and Fe^{2+} no sharp features were observed which would indicate strong isolated transitions resulting in ionization, although a factor of 2 increase in the Fe^{2+} cross section had been predicted based on preliminary calculations (as part of the work reported in Ref. 26). A very significant contribution is found from excitation autoionization for Fe^{5+} and Fe^{6+}, in good agreement with detailed calculations. Excitation autoionization is also predicted to dominate ionization of Fe^{15+}, which is Na-like. Confidence in this prediction is based on fair agreement between experiment[46] and theory[47] in other members of the Na isoelectronic sequence, but experimental results have only been published for charge states up to Si^{3+}. Another approach to the problem involves comparative studies along the Fe isonuclear sequence, and it has been predicted that excitation autoionization will be less important for Fe charge states lower than $+15$, with only a few percent contribution predicted[44] for ionization of Ar-like Fe^{8+}. It is indeed observed that excitation autoionization is a relatively minor effect for Fe^{9+}, but it is clear that such general rules will not suffice if accurate cross-section predictions are desired, and that measurements for even higher charge states of Fe will be necessary to test predictions.

V. RATE COEFFICIENTS

Since a number of important applications for these measurements require ionization rate coefficients rather than cross sections, the present results and the published cross-section measurements for Fe^+ and Fe^{2+} have been utilized to calculate ionization rate coefficients. The calculations were performed using a program developed for this purpose by the Controlled Fusion Atomic Data Center at Oak Ridge National Laboratory. Rate coefficients for electron-impact ionization may be derived from cross sections (assuming a Maxwellian electron energy distribution) through the relation

$$\alpha(T)=\frac{1}{(\pi m_e)^{1/2}}\frac{2}{(kT)^{3/2}}\int_0^\infty \sigma(E)Ee^{-(E/kT)}dE\ . \qquad (4)$$

In order to minimize errors in the calculated rate coefficients in the present study due to the finite energy range over which cross sections have been measured, each data set was extrapolated upward in energy to 10 keV by scaling the $(\ln E)/E$ energy dependence predicted in the Bethe-Born approximation from the highest-energy experimental point. The rate coefficients were calculated by the method of Gaussian integrals[48] and logarithmic inter-

TABLE III. Rate coefficients (in units of 10^{-10} cm^3/s) at selected values of kT (in eV) derived from cross-section measurements. Fe^+ and Fe^{2+} data for use in these calculations are taken from Refs. 24 and 19, respectively.

kT (eV)	(Rate coefficients 10^{-10} cm^3/s) Fe^+	Fe^{2+}	Fe^{5+}	Fe^{6+}	Fe^{9+}
10.0	78.7	11.4	0.0	0.0	0.0
20.0	214.1	61.9	1.0	0.2	0.0
30.0	311.9	119.9	5.0	1.4	0.0
40.0	383.6	171.9	12.6	4.6	0.1
55.0	460.8	236.3	26.2	11.2	0.4
75.0	530.4	301.9	44.0	21.0	1.4
100.0	587.0	361.8	63.5	32.9	3.0
140.0	640.6	426.8	88.4	49.4	5.8
200.0	679.9	485.6	114.7	68.4	9.9
300.0	700.3	536.2	141.0	89.2	15.5
450.0	694.5	567.4	160.0	105.7	21.5
650.0	668.4	578.6	169.1	114.3	26.2
1000.0	617.2	571.6	169.0	115.2	29.7
1400.0	566.9	550.9	162.2	109.9	30.4
1900.0	518.2	519.0	152.9	103.1	29.1
2500.0	476.1	476.9	144.6	98.2[a]	26.7
3000.0	451.0	440.0	140.5	95.5[a]	24.7

[a]These values differ slightly from results obtained utilizing the fitting parameters of Table IV. Imperfections in the fit at the 5% level were caused by the limited number of fitting parameters.

polation was used to obtain estimates of the cross section at the required abscissa values. Both the step size of the integration and the order of the interpolation function were optimized for convergence and computational speed. The calculations were carried out for Maxwellian electron distributions having values of kT from 10 to 3000 eV. This corresponds to an electron temperature range of approximately $10^5 < T < 3.5 \times 10^7$ K. Tabulated rate coefficients at selected energies are included in Table III for each ion, and rate coefficient curves are plotted in Fig. 5. Fitting parameters for these rate coefficients are discussed in the Appendix.

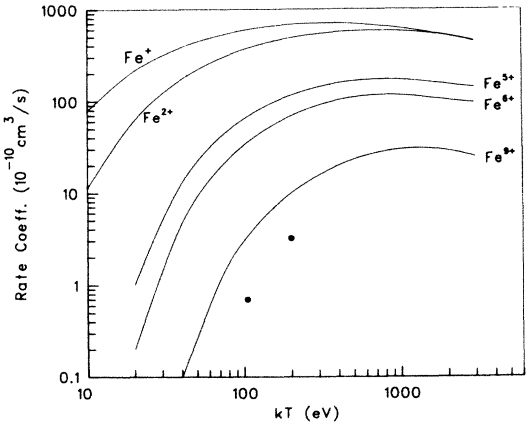

FIG. 5. Comparison of rate coefficients for electron-impact ionization of Fe ions. The solid curves are based on crossed-beam measurements of ionization cross sections; the Fe^+ and Fe^{2+} data are from Refs. 25 and 19, respectively. The filled circles are rate-coefficient measurements for Fe^{9+} from Refs. 48 and 49.

A. Comparisons with previous measurements and calculations

The only direct measurements of ionization rate coefficients for Fe ions of which we are aware are by Brooks *et al.*[48,49] based on time histories of emission lines in a small θ-pinch plasma. The two values reported for Fe^{9+} are plotted in Fig. 5 (filled circles). These results are somewhat model dependent, and no absolute error is reported. Although measurements at two temperatures ($kT_e = 105$ and 200 eV) were published, the $kT_e = 105$ result is derived from the $kT_e = 200$ measurement by assuming a shape for the rate coefficient as a function of temperature. Comparison with the present data indicate that the plasma rate coefficient measurement is lower than the present Fe^{9+} rate coefficient by at least a factor of 3 at 200 eV.

Rate coefficients can be calculated from the semiempirical Lotz ionization cross-section formula by convolution of a Maxwellian electron distribution with the ionization formula.[8] A comparison of these calculations with rate coefficients derived from crossed-beam experiments at temperatures in the 100—200-eV range reveal patterns similar to those observed in comparing the corresponding cross-section curves. For Fe^+, the Lotz rate coefficients are factors of 2—3 larger than experiment. Agreement is somewhat better for Fe^{2+}, where Lotz results are within 20% of the experimental results. Fe^{5+} and Fe^{6+}, with large contributions to the measured cross sections from indirect ionization, are underestimated by the Lotz formula by approximately factors of 2. For Fe^{9+} experiment and theory are again in better agreement, and most of the difference can be accounted for by the effects of metastable ions in the incident ion beam.

TABLE IV. Rate-coefficient fitting parameters. All parameters are in units of 10^{-11} cm^3/s. Rate coefficients in the range $10 < kT < 3000$ eV may be calculated using these parameters in a Chebyshev polynomial expansion, or through Clenshaw's algorithm (see Appendix).

	Rate coefficient fitting parameters (10^{-11} cm^3/s)						
Ion	a_0	a_1	a_2	a_3	a_4	a_5	a_6
Fe^+	8785.0	2100.0	−2002.0	−261.2	263.5	22.34	−5.619
Fe^{2+}	6628.0	2757.0	−1155.0	−616.5	131.3	2.630	−33.20
Fe^{5+}	1701.0	925.4	−167.6	−286.1	22.23	62.95	−2.591
Fe^{6+}	1111.0	642.0	−66.90	−201.0	−2.533	57.73	12.78
Fe^{9+}	254.3	169.2	16.08	−49.39	−24.90	3.787	5.265

VI. SUMMARY

Cross sections have been presented for ionization of Fe^{5+}, Fe^{6+}, and Fe^{9+} by electron impact, and modifications to the experimental apparatus that enabled us to utilize the crossed-beam method for these high charge states have been described. Distorted-wave calculations for direct ionization of ground-state ions at 60—70% below the experimental results near the peak cross sections due to additional contributions of excitation autoionization (for Fe^{5+} and Fe^{6+}) or the effects of metastable ions in the experiment (for Fe^{9+}). Ionization rate coefficients have been calculated based on the present results and previous measurements for Fe^+ and Fe^{2+}, and fitting parameters are listed to allow the simple calculation of rate coefficients over a wide range of temperatures based on these measurements. Rather poor agreement is found with previous θ-pinch rate coefficient measurements and mixed agreement is reported with results from the simple Lotz rate-coefficient formula.

The present experiment illustrates that, in a given isonuclear sequence, different mechanisms may contribute to total ionization over a relatively short span of charge states. Simple scaling models are not adequate to predict such behavior and detailed calculations, such as those in the accompanying paper, combined with benchmark experiments appear to be required to obtain accurate cross section predictions for an extensive system of ions.

ACKNOWLEDGMENTS

The authors acknowledge valuable conversations with R. A. Phaneuf, M. Pindzola, D. C. Griffin, C. Bottcher, and D. H. Crandall during this project. H. T. Hunter developed the rate-coefficient calculation and fitting program, and assisted in its present application. The technical assistance of J. W. Hale in the maintenance of the apparatus is also acknowledged. This work was supported by the Office of Fusion Energy, U.S. Department of Energy, under Contract No. DE-AC05-840R21400 with Martin Marietta Energy Systems, Inc.

APPENDIX: FITTING PARAMETERS FOR RATE COEFFICIENTS

In addition to the tabulated values in Table III, a set of fitting parameters are included in Table IV which allows the user to calculate the rate coefficient at any value of kT from 10 to 3000 eV for any of the ions included here. The coefficients a_0—a_6 in Table IV were fitted following the method reported by Cox and Hayes[50] and may be utilized in a direct expansion through Chebyshev polynomials of the first kind[51,52] [$T_r(x)$] to obtain rate coefficients through the formula

$$\alpha(kT)=\tfrac{1}{2}a_0+\sum_{r=1}^{6}a_r T_r(x)\ . \tag{A1}$$

The coefficients in Table IV may also be converted, using Clenshaw's algorithm,[53] to modified coefficients (b_n) which give the rate coefficient directly. A complete analytic expansion of the Clenshaw coefficients results in the same expression as the summed Chebyshev polynomials, but calculation of rate coefficients through the Clenshaw algorithm is faster and easier than calculating the rather cumbersome polynomials. For the range $10 < kT < 3000$ eV, the rate coefficient α (cm^3/sec) is expressed in terms of the Clenshaw coefficients by the simple expression

$$\alpha(kT)=\tfrac{1}{2}(b_0-b_2)\ , \tag{A2}$$

where b_0 and b_2 are found by sequentially calculating $b_6, b_5, b_4, \ldots$ according to the relations

$$b_n=2xb_{n+1}-b_{n+2}+a_n\ . \tag{A3}$$

In Eq. (A3), $n=6,5,4,\ldots,0$ and $b_8=b_7=0$. The coefficients a_6—a_0 are listed in Table IV and the reduced energy x is given by

$$x=(\ln kT-5.154)/2.852\ . \tag{A4}$$

The sequential calculation of b_n's is necessary since each b_n except b_6 and b_5 depend on b_{n+1} and b_{n+2}.

*Permanent address: Institut für Kernphysik, Justus-Liebig-Universität Giessen, D-6300 Giessen, Federal Republic of Germany.

[1]D. E. Post, in *Physics of Ion-Ion and Electron-Ion Collisions* (Plenum, New York, 1983), pp. 37–99.

[2]A. Dalgarno, *ibid.* pp. 1–36.

[3]D. Palumbo, Phys. Scr. **23**, 69 (1981).

[4]David H. Crandall, Nucl. Instrum. Methods **214**, 129 (1983).

[5]D. E. Post, R. V. Jensen, C. B. Tarter, W. H. Grasberger, and W. A. Lokke, At. Data Nucl. Data Tables **20**, 397 (1977).

[6]Wolfgang Lotz, Z. Phys. **206**, 205 (1967).

[7]Wolfgang Lotz, Z. Phys. **216**, 241 (1968).

[8]Wolfgang Lotz, Z. Phys. **220**, 466 (1969).

[9]O. Bely, J. Phys. B **1**, 23 (1968).

[10]S. O. Martin, B. Peart, and K. T. Dolder, J. Phys. B **1**, 537 (1968).

[11]D. H. Crandall, R. A. Phaneuf, B. E. Hasselquist, and D. C. Gregory, J. Phys. B **12**, L249 (1979).

[12]D. H. Crandall, R. A. Phaneuf, R. A. Falk, D. S. Belic, and G. H. Dunn, Phys. Rev. Rev. A **25**, 143 (1982).

[13]A. Müller, E. Salzborn, R. Frodl, R. Becker, H. Klein, and H. Winter, J. Phys. B **13**, 1877 (1980).

[14]D. C. Griffin, C. Bottcher, M. S. Pindzola, S. M. Younger, D. C. Gregory, and D. H. Crandall, Phys. Rev. A **29**, 1729 (1984).

[15]C. Achenbach, A. Müller, E. Salzborn, and R. Becker, J. Phys. B **17**, 1405 (1984).

[16]R. A. Falk, G. H. Dunn, D. C. Griffin, C. Bottcher, D. C. Gregory, D. H. Crandall, and M. S. Pindzola, Phys. Rev. Lett. **47**, 494 (1981).

[17]For a recent summary of published work, see G. H. Dunn, in *Electron Impact Ionization* (Springer-Verlag, Vienna, 1985), pp. 277–318.

[18]M. J. Diserens, M. F. A. Harrison, and A. C. H. Smith, Abstracts of the Sixteenth National Atomic and Molecular Physics Conference, University College, London, 1984 (unpublished).

[19]D. W. Mueller, T. J. Morgan, G. H. Dunn, D. C. Gregory, and D. H. Crandall, Phys. Rev. A **31**, 2905 (1985).

[20]A. Müller, K. Tinschert, Ch. Achenbach, E. Salzborn, R. Becker, and M. S. Pindzola, Phys. Rev. Lett. **54**, 414 (1985).

[21]D. C. Gregory and A. M. Howald, Phys. Rev. A **34**, 97 (1986).

[22]See, for example, G. A. Doschek, in *Autoionization* (Plenum, New York, 1985), pp. 171–256.

[23]M. R. C. McDowell, in *Atomic and Molecular Processes in Controlled Thermonuclear Fusion* (Plenum, New York, 1980), pp. 1–14.

[24]Einar Hinnov, *ibid.*, pp. 449–470.

[25]R. G. Montague, M. J. Diserens, and M. F. A. Harrison, J. Phys. B **17**, 2085 (1984).

[26]M. S. Pindzola, D. C. Griffin, and C. Bottcher, following paper, Phys. Rev. A **34**, 3668 (1986).

[27]K. T. Dolder and B. Peart, Rep. Prog. Phys. **39**, 693 (1976).

[28]D. H. Crandall, R. A. Phaneuf, and P. O. Taylor, Phys. Rev. A **18**, 1911 (1978).

[29]D. C. Gregory, P. F. Dittner, and D. H. Crandall, Phys. Rev. A **27**, 724 (1983).

[30]M. F. A. Harrison, Brit. J. Appl. Phys. **17**, 371 (1966).

[31]M. F. A. Harrison, in *Methods of Experimental Physics* (Academic, New York, 1968), Vol. 7, Part A, pp. 95–116.

[32]F. Brouillard and P. Defrance, Phys. Scr. **3**, 801 (1983).

[33]D. F. Dance, M. F. A. Harrison, and A. C. H. Smith, Proc. R. Soc. London, Ser. A **290**, 74 (1966).

[34]M. L. Mallory and D. H. Crandall, IEEE Trans. Nucl. Sci. **NS-23**, 1069 (1976).

[35]F. W. Meyer, Nucl. Instrum. Methods Phys. Res. B **9**, 532 (1985).

[26]P. O. Taylor, K. T. Dolder, W. E. Kauppila, and G. H. Dunn, Rev. Sci. Instrum. **45**, 538 (1974).

[37]P. O. Taylor, thesis, University of Colorado, 1972, available through University Microfilms, Ann Arbor, Michigan.

[38]D. S. Belić, R. A. Falk, G. H. Dunn, D. Gregory, C. Cisneros, and D. H. Crandall, Bull. Am. Phys. Soc. **27**, 49 (1981).

[39]J. N. Fox, R. L. Fitzwilson, and E. W. Thomas, J. Phys. E **3**, 36 (1970).

[40]Joachim Fricke, Alfred Müller, and Erhard Salzborn, Nucl. Instrum. Methods **175**, 379 (1980).

[41]D. H. Crandall, J. A. Ray, and Carmen Cisneros, Rev. Sci. Instrum. **46**, 562 (1975).

[42]S. M. Younger, *Atomic Data Fusion* (Oak Ridge National Laboratory, Tennessee, 1981), Vol. 7, p. 190.

[43]Enrico Clementi and Carlo Roetti, At. Data Nucl. Data Tables **14**, 177 (1974).

[44]S. M. Younger, J. Quant. Spectrosc. Radiat. Transfer **29**, 61 (1983).

[45]K. J. LaGattuta and Y. Hahn, Phys. Rev. A **24**, 2273 (1981).

[46]D. H. Crandall, R. A. Phaneuf, R. A. Falk, D. S. Belić, and G. H. Dunn, Phys. Rev. A **25**, 143 (1982).

[47]D. C. Griffin, C. Bottcher, and M. S. Pindzola, Phys. Rev. A **25**, 154 (1982).

[48]R. L. Brooks, R. U. Datla, and Hans R. Griem, Phys. Rev. Lett. **41**, 107 (1978).

[49]R. L. Brooks, R. U. Datla, A. D. Krumbein, and Hans R. Griem, Phys. Rev. A **21**, 1387 (1980).

[50]M. G. Gox and J. G. Hayes, U.K. National Physical Laboratory report No. NAC 26, 1973 (unpublished).

[51]See, for example, Jon Mathews and Robert L. Walker, *Mathematical Methods of Physics* (Benjamin, New York, 1970), pp. 351–353.

[52]See, for example, *Handbook of Mathematical Functions,* edited by Milton Abramowitz and Irene A. Stegun (Dover, New York, 1970).

[53]C. W. Clenshaw, Math. Tables Comput. **9**, 118 (1955).